Account

Nanocrystals and Their Biomedical Applications

Young-wook Jun, Jung-tak Jang, and Jinwoo Cheon*

*Department of Chemistry, Yonsei University, Seoul 120-749, Korea. *E-mail: jcheon@yonsei.ac.kr*
Received March 22, 2006

Shape controlled synthesis of inorganic nanocrystals is one of the important issues in materials chemistry due to their novel shape dependent properties. Although various shapes of nanocrystals have been developed, a systematic account on the shape control of these nanocrystals still remains an important subject in materials chemistry. In this article, we will overview the recent developments in the geometrical shape evolution of semiconductor and metal oxide nanocrystals obtained by nonhydrolytic synthetic methods. Many structurally unprecedented motifs have appeared as zero-dimesional (D) polyhedrons, one-D rods and wires, two-D plates and prisms, and other advanced shapes such as branched rods, stars, and inorganic dendrites. Important parameters which determine the geometrical shapes of nanocrystals are also illustrated. In addition, as a possible application of such nanocrystals for biomedical sciences, we further describe their utilizations for cancer diagnosis through nanocrystal-assisted magnetic resonance imaging (MRI).

Key Words : Nanocrystals, Shape control, Anisotropic nanostructures, Nano-MRI

Introduction

Nanocrystals are the important components for next-generation nanoscale devices,[1] and the successful operation of these devices will be easily accomplished by using nanocrystals with distinct sizes and shapes. By assembling and patterning nanocrystals in a manner similar to assembling "Lego" blocks, the fabrication of next generation devices that are extremely fast, efficient, and small can be possible.[2]

It has been found that size and shape of nanocrystals are key factors for the determination of their unique chemical and physical properties. Bulk materials have their own characteristics and innate properties such as color, phase transition temperature, and band-gap energy. However, nanocrystalline materials no longer retain such bulk properties and exhibit unprecedented novel phenomena associated with nanoscale dimension. For example, bulk gold has golden color and melts at ~1,064 °C. In contrast, under nanoscale regime, color of gold can be tuned from red, to deep violet, and to blue by controlling their size and shape.[3] Similarly, its melting point is significantly decreased to ~350 °C at the size of ~1.6 nm.[4] The band-gap energy of CdSe nanocrystals gradually increases from 1.75 eV to 2.6 eV as their size decreases from 12 nm to 1.2 nm as exemplified,[5] the size and shape of nanocrystals now plays as crucial parameters to determine their new nanoscale chemical and physical properties. Such novel phenomena of nanocrystals are interesting and valuable to be further investigated. Once we learn methods to control the size and shape of nanocrystal precisely, therefore, their chemical and physical properties can be tailored as desired.

During past decades, researchers have pursued to have an

Young-wook Jun earned his B.S. degree in chemistry from Yonsei University (1999) and his Ph. D. degree in chemistry from the Korea Advanced Institute of Science and Technology (KAIST) (2005), where he studied the controlled synthesis and assembly of colloidal inorganic nanocrystals under the guidance of Professor Sang Youl Kim and Professor Jinwoo Cheon. Currently, he is carrying out postdoctoral studies as a member of Professor Cheon's group at Yonsei University. He is a recipient of the Honorable Mention Award of the IUPAC Prize for Young Chemists (2005). His current research focuses on the development of smart inorganic nanocrystal-biomolecule hybrid systems for biomedical imaging and sensor applications.

Jung-tak Jang was born in 1977 in Ulsan, Korea. He earned his B.S. degree in chemistry from Sogang University in 2005 and now is a first year graduate student pursuing his Ph.D. degree at Yonsei University under the supervision of Prof. Jinwoo Cheon. His current research interests are the size controlled synthesis of various magnetic nanocrystals and tailored surface modification chemistry for biological studies.

Jinwoo Cheon is a Professor of Chemistry at Yonsei University and Head of the Nanomaterials Division of the Nano-Medical National Core Research Center of Korea. He received his B.S. and M.S. degrees in chemistry from Yonsei University in Seoul, Korea. He then moved to the University of Illinois, Urbana-Champaign where he earned his Ph.D. in organometallics and materials chemistry from Prof. G. Girolami in 1993. After receiving post-doctoral training at the University of California, Berkeley, with Prof. J. Arnold and Dr. E. Bourret in the field of molecular precursor chemistry for semiconducting materials and also at UCLA with Prof. J. Zink studying the photochemistry of inorganic materials, he joined the Korea Advanced Institute of Science and Technology (KAIST) as an assistant professor in 1998. In 2002, he moved to Yonsei University. Professor Cheon was elected as a junior member of the Korean Academy of Science and Technology in 2003 and is a recipient of the Korean Chemical Society Award in Inorganic Chemistry (2004), the National Science Prize for Junior Faculty (2002), and the Korean Chemical Society-Wiley Young Chemist Award (2001). His research areas include the fabrication and shape control of inorganic nanocrystals, nanoscale opto-magnetics, and their applications for biomedical sciences.

efficient synthetic route of well-defined inorganic nanocrystals. Various synthetic approaches have been adopted for the size and shape controlled nanocrystal growth, which include gas-phase vapor-liquid-solid (VLS) method and thermal evaporation,[6-14] crystal growth in a nanoporous solid template,[15] aqueous colloidal nanocrystal growth in a structured micelle,[16] and nonhydrolytic colloidal synthesis.[17-50] Among these methods, nonhydrolytic colloidal approach is proven to be a convenient and reproducible route for the fabrication of nanocrystals with excellent crystallinity and a controlled size and shape. In such a method, typically, molecular precursors, which usually contain key elements for desired nanocrystalline materials, are injected into a hot (~100–350 °C) organic solvent with capping molecules, which induces i) a rapid increase of the monomer concentration, ii) nanocrystal growth through aggregation of the monomers, and iii) surface passivation of the resulting nanocrystals with capping molecules. Moreover, this method has several controllable synthetic aspects: i) facile separation between nucleation and growth stages, ii) control of growth parameters such as the choice of the molecular precursor and capping molecules, the reaction temperature, and the growth time.

Early investigations of the nanocrystal fabrication have focused on the synthesis of zero-dimensional isotropic shaped nanocrystals such as spheres, cubes, tetrahedrons, and tetradecahedrons.[5,17-20] Since monodisperse CdSe nanospheres were synthesized through a molecular precursor injection method in a hot surfactant solution by Bawendi and coworkers,[5] a variety of spherical nanocrystals of semiconductors, metal oxide, and metal nanocrystals have been synthesized (Figure 1A). Researchers have further explored anisotropic one-dimensional shapes which exhibit novel optical and magnetic properties arising from shape effects (Figure 1B). Included in this group are rods and wires of group II-VI semiconductors (*e.g.* CdS,[21-23] CdSe,[21,24-26] CdTe,[11,27,28] ZnSe[29]), III-V semiconductors (GaP,[30] InP[31]), IV semiconductor (Ge[32]), other semiconductors (PbS,[33] PbSe,[34,35] MnS[36,37]), and transition metal oxides (*e.g.* ZnO,[38,39] TiO_2,[39-41] $W_{18}O_{49}$,[41,42] Mn_3O_4,[41,43] V_2O_5,[39] $BaTiO_4$,[44] and Fe_3O_4[45]). Two dimensional discs and plates with polygon shapes were also synthesized: Cu_2S[46] and NiS[47] nanodiscs, Co metal nanodiscs,[48,49] Gd_2O_3 nanodiscs,[50] and Fe_2O_3 trigonal prisms[45] have been recently reported (Figure 1C). Besides such primitive shapes of inorganic nanocrystals, advanced shapes of nanocrystals have been developed. Multipod structures of semiconductors (*e.g.* CdS,[23] CdSe,[25] CdTe,[27] MnS,[36] ZnSe[29]) including bipods, tripods, and tetrapods, and star-shaped PbS nanocrystals,[33] and dendritic CdSe[25] and CdTe[27] nanocrystals are the examples of such cases. Although there are increasing number of examples of nanocrystals with anisotropic shapes from simple one-dimensional rods and wires to advanced multipods and stars, the reports on their shape-guiding mechanism are very limited. To obtain more advanced-structured nanocrystals and to have the ability to control the nanocrystal shape as desired, the unraveling and systematic understanding of shape-guiding processes are necessary.

In this article, we review the recent progresses in the development of colloidal nanocrystals with various shapes. In particular, we focus on the semiconductor and metal oxide nanocrystals synthesized through the nonhydrolytic chemical route, with an emphasis on the possible growth mechanisms and current achievements of nanocrystal shape controls. Critical parameters for the nanocrystal shape determination are discussed through the case studies of nanocrystal growths of various semiconductors (*e.g.* CdS,[23] MnS,[36] $Cd_{1-x}Mn_xS$,[36] GaP,[30] PbS[33]) and transition metal oxides[41] (*e.g.* TiO_2, $W_{18}O_{49}$, Mn_3O_4).

Shape Guiding Mechanism of Inorganic Nanocrystals

Nanocrystal formation can be simply understood as two step procedures: i) nucleation initiated by sudden increase of monomer concentration over super-saturation levels, and ii) the subsequent crystal growth from the seed with progressive consumption of monomers in solution. (Figure 2) The final geometry of nanocrystals is determined by several

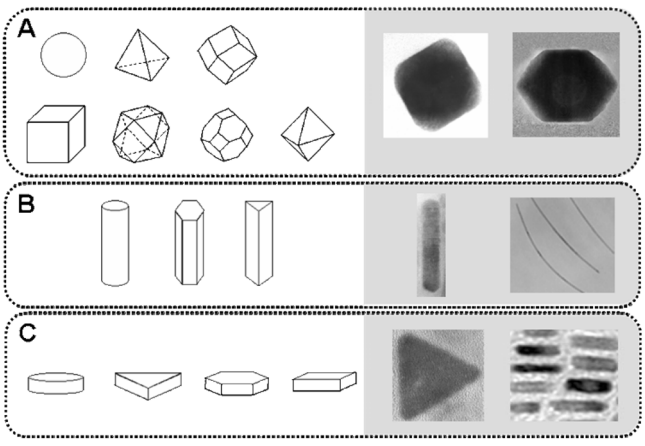

Figure 1. Representative geometrical motifs and TEM images of inorganic nanocrystals.

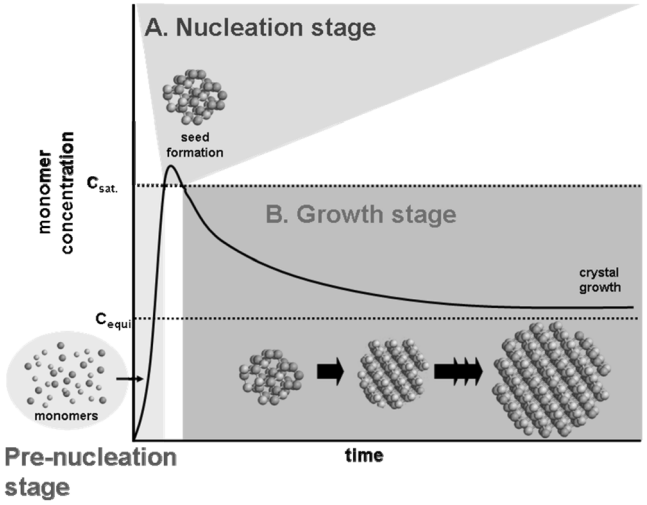

Figure 2. Nanocrystal growth diagram. (A) Nucleation stage, (B) growth stage.

parameters during these nucleation and growth processes. Initially, the crystalline phase of the seed at the nucleating stage is critical for the directing nanocrystal shapes due to its characteristic unit cell structure. Once nanocrystal seeds are formed with a specific crystalline phase, several other factors for controlling the subsequent growth processes will affect the final geometry of nanocrystals. Such key factors include the intrinsic surface energy of different crystallographic surfaces, the role of surface selective capping molecules, and the choice of the nanocrystal growth regime between thermodynamic and kinetic regimes.

Nucleation stage: crystalline phase effect. Nucleating seeds of nanocrystals can potentially have a variety of crystalline phases from isotropic structure of cubic to anisotropic structure of hexagonal or monoclinic. Among various crystalline phases, the stable phase of materials is highly dependent on its environments such as temperature and the choice of capping molecules. For example, by adjusting the initial temperature during the nucleation process, the crystalline phase of nanocrystals can be controlled. Once the crystalline phase is determined, the characteristic unit cell structure of the seeds strongly affects on the further nanocrystal growth processes. For example, an isotropic unit cell structure (*e.g.* cubic) of the seed generally induces the isotropic growth of nanocrystals from the seed, and therefore, zero-dimensional nanostructures are possible. In contrast, anisotropic unit cell structures of the seed can induce anisotropic growth along crystallographically reactive surfaces and therefore anisotropic shapes of nanocrystals are expected. The growth of MnS nanocrystals can be a good example of such case.[36] MnS crystals possess diverse crystallographic structures from isotropic rock-salt structure and zinc blende to anisotropic wurtzite (Figure 3). It is known that the rock salt structure is more stable at high temperature (> 200 °C), whereas the wurtzite structure is preferred at temperatures below 200 °C.[51,52] At high temperature (~200 °C), the seed of rock salt structured MnS induces isotropic growth along eight {111} directions, and 30 nm sized nanocubes are easily observed after the injection of the molecular precursor, $Mn(S_2CNEt_2)_2$, into a hot solution containing hexadecylamine capping molecules (Figure 3A). In contrast, at low temperature (~120 °C), the nucleation of the hexagonal wurtzite structure results in anisotropic growth along the *c*-axis of wurtzite structures and therefore thin nanowires of 2 nm in diameter with an aspect ratio of ~80 are obtained (Figure 3B).

Similar crystalline phase effects of the seeds can be observed in the case of CdS nanocrystal growth.[23] CdS has two distinct crystalline phases: an isotropic zinc blende is stable below 250 °C and hexagonal wurtzite is preferred at higher temperature (~300 °C).[53] At high temperature, the exclusive formation of one-dimensional CdS rods is observed from high temperature stable wurtzite structured seeds, as similarly seen in the MnS nanowire growth (Figure 4A). However, at lower temperatures, the formation of tetrahedral shapes of zinc blende seeds truncated with four {111} faces is clearly facilitated. The subsequent epitaxial growth of wurtzite pods along the *c*-axis from the four equivalent {111} faces of the seed results in the formation of CdS tetrapods (Figure 4B). High resolution transmission electron microscopic (HR-TEM) analyses show the crystalline phase effect on these CdS monorods and multipods (Figure 4C, D). The monorods prepared at high temperature have hexagonal wurtzite structures (Figure 4C). In contrast, the HRTEM image of bipods prepared at lower temperatures indicates that the core is of cubic-phased zinc blende structure with tetrahedral geometry and a separation angle of ~109.5° between arms of the bipods (Figure 4D).

Besides such temperature mediated crystalline phase control of seeds, the choice of capping molecules can be a means of controlling the crystalline phase of seeds. Since the capping molecules dynamically bind to the crystal surface during the nucleation and crystal growth processes, the conformation of crystal structure is highly affected by the identity of the capping molecules. For example, GaP have two distinct crystalline phases that are in rotational iso-

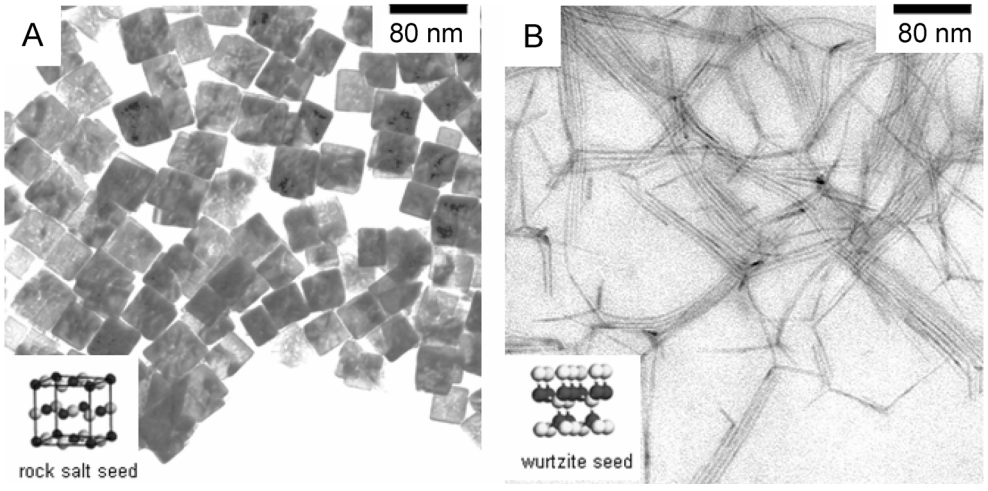

Figure 3. Crystalline phase effect on shape determination of MnS nanocrystals. (A) Nanocubes obtained at ~200 °C, (B) nanowires obtained at ~120 °C.

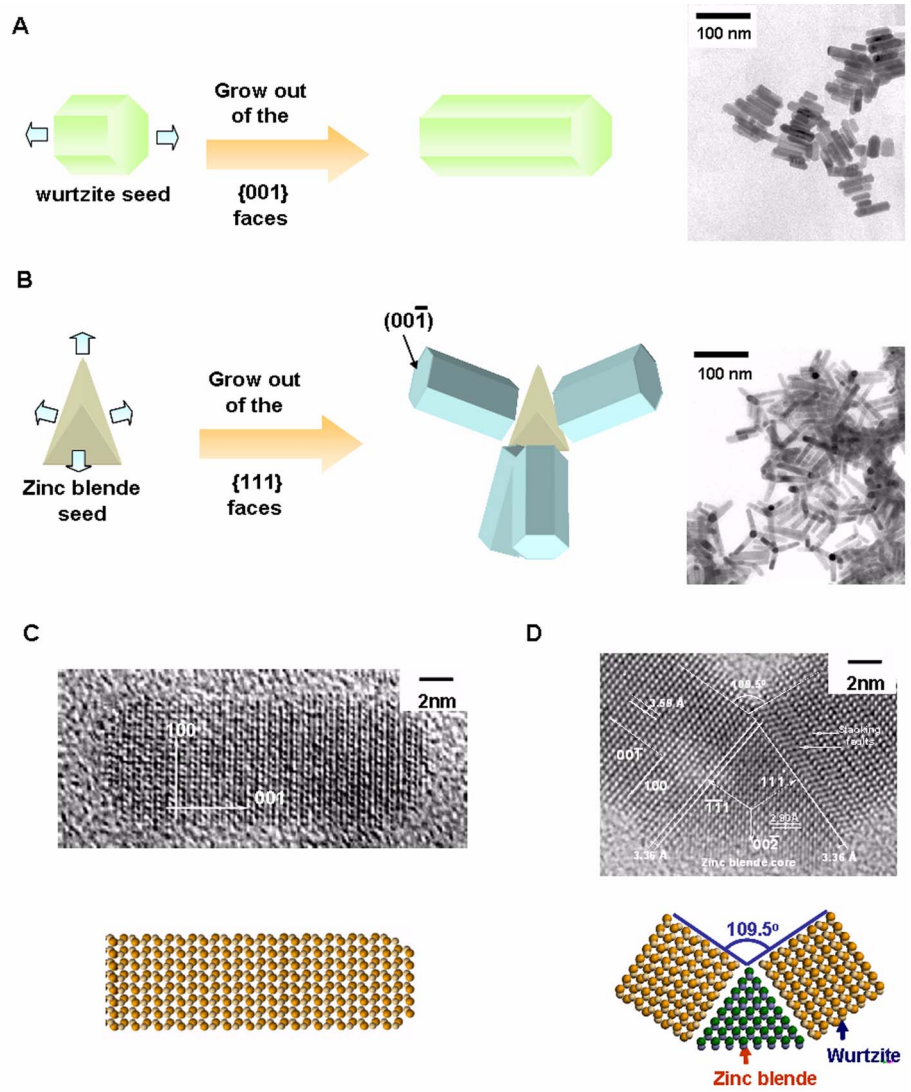

Figure 4. CdS nanocrystal growth. (A) Monorods from hexagonal wurtzite seeds, (B) tetrapods from zinc blende seeds, (C, D) HRTEM images of (C) a monorod and (D) a bipod.

merism: the zinc blende phase which is a staggered conformation with <111> directions while the wurtzite phase is an eclipsed conformation with <001> directions (Figure 5A, B). Zinc blende GaP is a thermodynamically stable phase that is sterically favored.[54] Wurtzite GaP is a kinetically stable phase that is favored due to the electrostatic interaction between vicinal gallium and phosphine atoms when GaP monomers approach the crystal surface.[54] The energy difference between these two phases is subtle and the control of the steric effect of GaP monomer molecules can have a significant affect on the conformation of crystal structures.[30] When sterically bulky tertiary amines (*e.g.* trioctylamine) are used as capping molecules, staggered conformation is highly favored due to the large steric hindrance between tertiary amine capping molecules and the crystal surface (Figure 5C). Therefore, formation of zinc blende GaP nanospheres results (Figure 5E). However, when sterically less hindered primary amines (*e.g.* hexadecylamine) are used, the steric energy difference between eclipsed and staggered conformations is diminished (Figure 5D). Therefore, steric effects on determining the binding geometry of incoming monomers are now minor and electronic effects play a major role. This facilitates the formation of the kinetically stable wurtzite GaP and further induces the formation of rod-shaped nanocrystals elongated with *c*-axis under the kinetic growth regime induced by a high monomer concentration (Figure 5F). The GaP nanocrystals obtained exhibit unique shape-dependent optical features originating from quantum mechanical effects. The absorption spectra show strong shoulders (3.48 and 3.46 eV for spheres and rods, respectively) and shallow tails that are attributed to direct and indirect transition, respectively.[55] The photoluminescence maximum is 2.94 eV for spheres corresponding to the direct transition of 8 nm GaP, while red shift (2.79 eV) is observed for rods (8 nm × 45 nm), which may arises from shape anisotropy.[56]

Growth stage: intrinsic surface energy and selective adhesion of capping molecules. After the crystalline phase

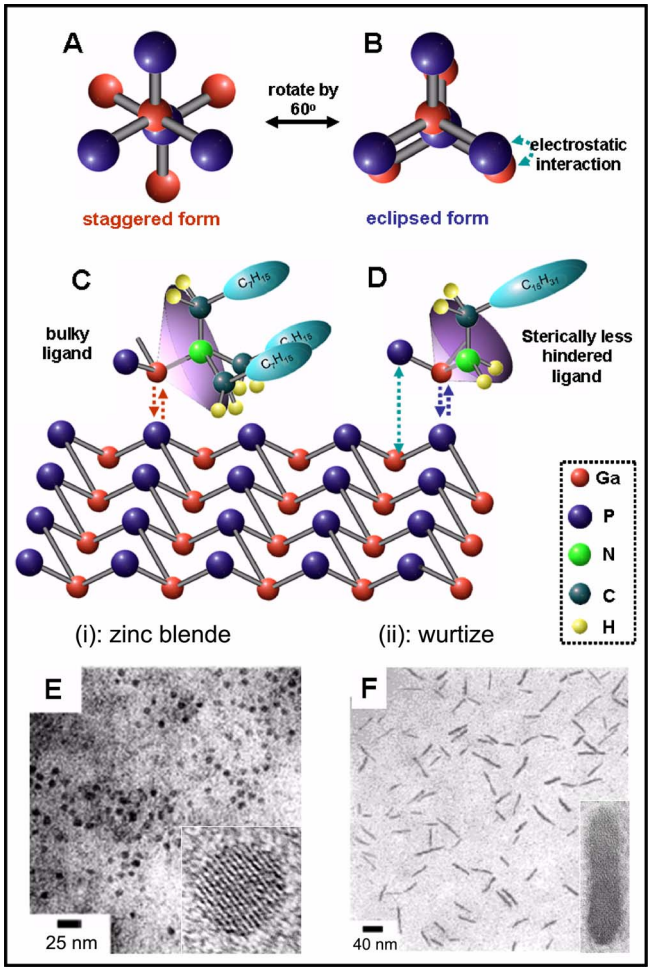

Figure 5. Capping molecule mediated seed formation of GaP nanocrystals. (A) Staggered conformation of the zinc blende structures, (B) eclipsed structures of the wurtzite structure, (C) sterically favored seed formation under the use of trioctylamine, (D) electronically favored seed formation under the use of hexadecylamine, (E) zinc blende structured GaP nanospheres, (F) wurtzite structured GaP nanorods.

of nucleating seeds is determined, several parameters during the subsequent growth stages strongly govern the final shapes of nanocrystals. One of critical parameters influencing the growth patterns of nanocrystals is the surface energy of the crystallographic faces of the seed. Since the crystal growth rate is highly related to the nanocrystal surface energy, it is important to examine the surface energy related effects on the anisotropic growth of nanocrystals.

The anisotropic growth of anatase TiO_2 nanocrystals is driven by such intrinsic surface energy effect.[40] Anatase TiO_2 has tetragonal structures elongated along *c*-axis and the {001} faces have the highest surface energy with the maximum packing density and a large number of undercoordinated atoms. Such surface energy difference results in the significant growth rate differences between different crystallographic directions, since the growth rate is exponentially proportional to the surface energy.[57] The growth rate along the <001> directions is much faster compared to other directions, which result in the progressive elongation along

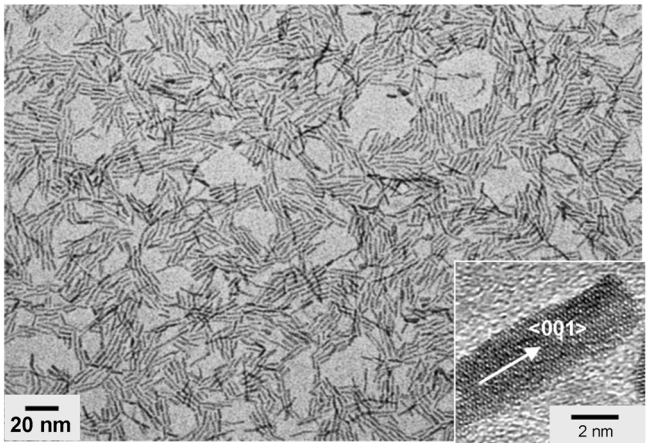

Figure 6. (A) TEM image of TiO_2 nanorods. (Inset) HRTEM image.

the <001> directions and formation of one-dimensional rod structures (Figure 6). Anisotropic rod growth of hexagonal wurtzite semiconductors including CdS,[21-23] CdSe,[21,24-26] CdTe,[21,27] ZnSe,[29] MnS,[36] and GaP,[30] can be also understood in a similar manner. The surface energy of {001} faces of the wurtzite structure is much larger than those of other faces such as {100} and {110} and induces unidirectional growth along the [001] direction.

The surface energy dependent shape control of nanocrystals can be elaborated by modulating the relative surface energies with the use of surface selective capping molecules. Rock salt phased PbS crystals generally nucleate as tetradecahedron seeds, exposing six {100} faces and eight {111} faces.[33] Since intrinsic surface energy of the {111} faces is higher than that of the {100} faces, relatively fast growth along the eight equivalent <111> directions from the tetradecahedron seeds results in the formation of cube-shaped nanocrystals. When the nanocrystals are synthesized through the thermal decomposition of molecular precursors $Pb(S_2CNEt_2)_2$ in a hot organic solution containing dodecylamine as nonselective capping molecules, cube-shaped PbS nanocrystals are obtained (Figure 7A). The use of dodecanethiol as capping molecules instead of dodecylamine allows the systematic shape evolution of PbS nanocrystals. The dodecanethiol molecules tend to selectively stabilize the {111} faces *via* μ^3-Pb_3-SR bridging bonds while they bind weakly to the {100} faces via a single bonding mode (Figure 8). Therefore, the surface energy of the {111} faces can selectively be lowered relative to that of the {100} faces. The cube-shapes of PbS nanocrystals are gradually changed to truncated octahedrons via truncated cubes, as the dodecanethiol concentration is increased. The increase in R factor (r_{100}/r_{111}, the ratio of the central distance of the {100} faces to that of the {111} faces) from 0.60 to 0.79 and 0.98 by increasing dodecanethiol concentration also reveals that the higher concentration of dodecanethiol blocks the growth on the {111} faces and facilitates the growth on the {100} faces (Figure 7B-D).

Growth stage: kinetic *vs.* thermodynamic nanocrystal growth. Another critical shape guiding parameter which is

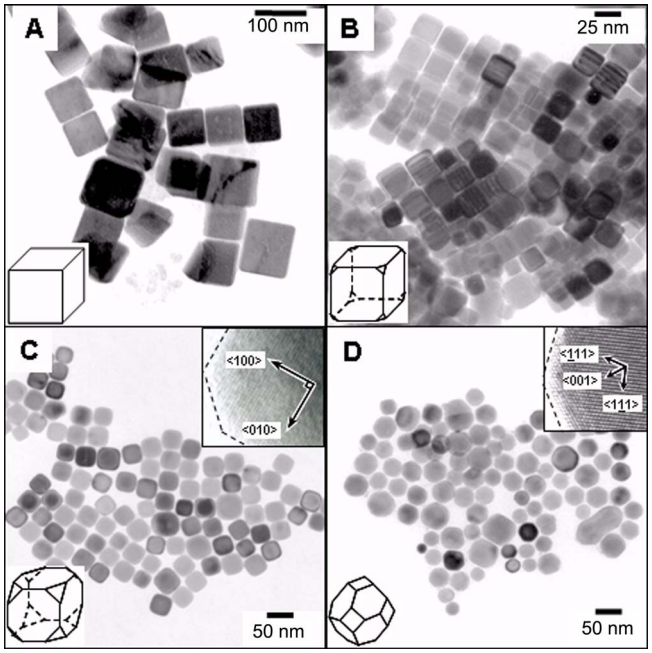

Figure 7. PbS nanocrystals. (A) Cubes, (B, C) truncated cubes, (D) tetradecahedrons. (Insets) HRTEM images of (C, inset) truncated cubes and (D, inset) tetradecahedrons.

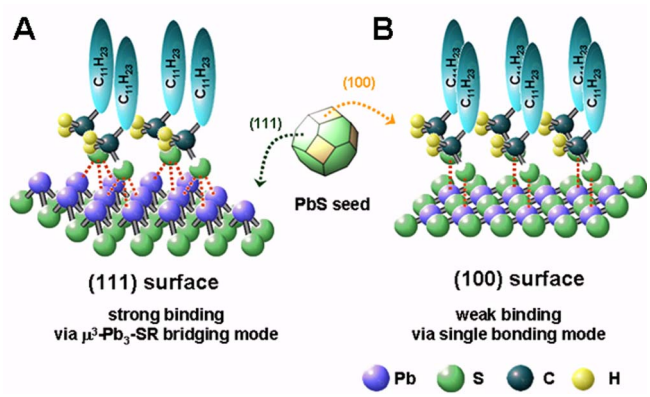

Figure 8. Binding modes of alkanethiols on PbS crystals. (A) μ^3-Pb_3-SR bridging mode on {111} surfaces, (B) single bonding mode on {100} surfaces.

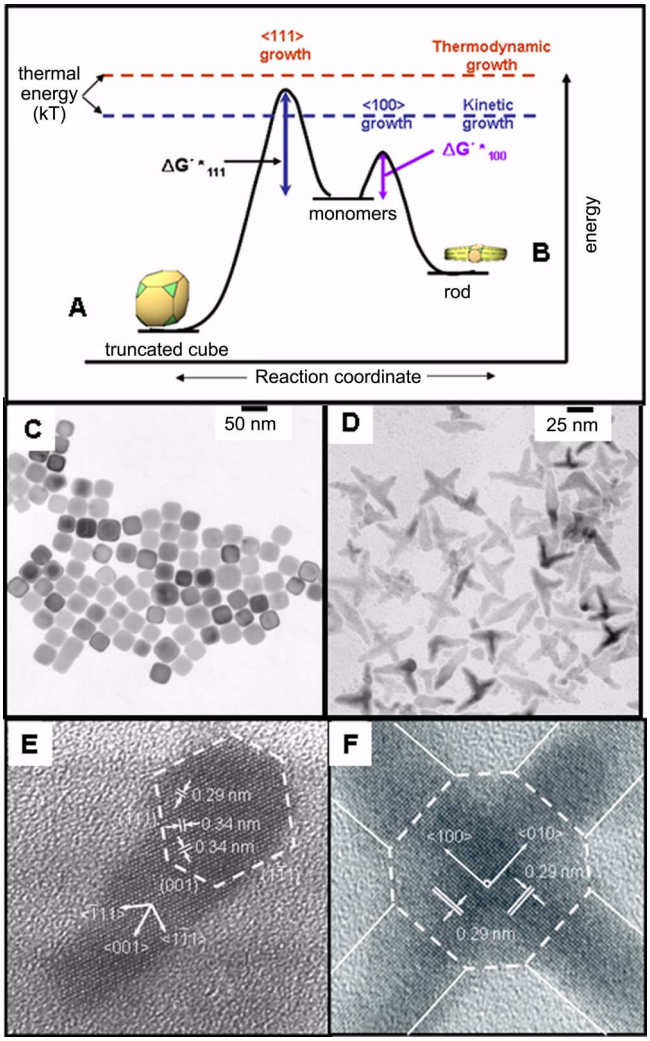

Figure 9. Growth regime dependent PbS nanocrystal shape control. (A, B) Growth pathways under (A) the thermodynamic regime ($kT > \Delta G^{\ddagger}_{111} > \Delta G^{\ddagger}_{100}$) and (B) the kinetic regime ($\Delta G^{\ddagger}_{111} > kT > \Delta G^{\ddagger}_{100}$). (C, D) TEM images of (C) thermodynamically induced truncated cube shapes of PbS, (D) kinetically induced mono- and multipods of PbS, (E, F) HRTEM image of (E) a monopod and (F) a tetrapod.

determined in the growth stage is the delicate balance between the kinetic and the thermodynamic growth regimes. Under the thermodynamic growth regime that is characterized by a sufficient supply of thermal energy (kT) and low flux of monomer, monomers isotropically grow from the nucleating seeds and therefore the formation of zero-dimensional structures (*e.g.* sphere) is preferred. Sphere is the thermodynamically most stable shape with the lowest overall surface energy. In contrast, under the non-equilibrium kinetic growth regime with a high flux of monomers, preferential anisotropic growth can be facilitated along the kinetically most favorable directions with low activation energy barriers.

The control of growth regime between kinetic *vs.* thermodynamic growth can be achieved by changing the reaction parameters such as the monomer concentration and the growth temperature.[19,20,26,29] The monomer concentration effects on the shape evolution of CdSe nanocrystals were extensively studied by Peng and coworkers.[26] At a low concentration of monomers at a fixed growth temperature, thermodynamically favorable-isotropic growth from the wurtzite seeds is preferred, which results in the formation of nanospheres. However, at a higher monomer concentration, kinetically favorable-anisotropic growth along the [00$\underline{1}$] direction of the wurtzite CdSe is favored, since the difference in growth rate between [00$\underline{1}$] direction and other directions is accentuated by increasing the monomer concentration.

The shape evolution of rock salt phased PbS nanocrystals provides a good example of the temperature effects on the choice of growth regime.[33] As described, PbS nucleates as tetradecahedron truncated with eight {111} faces and six

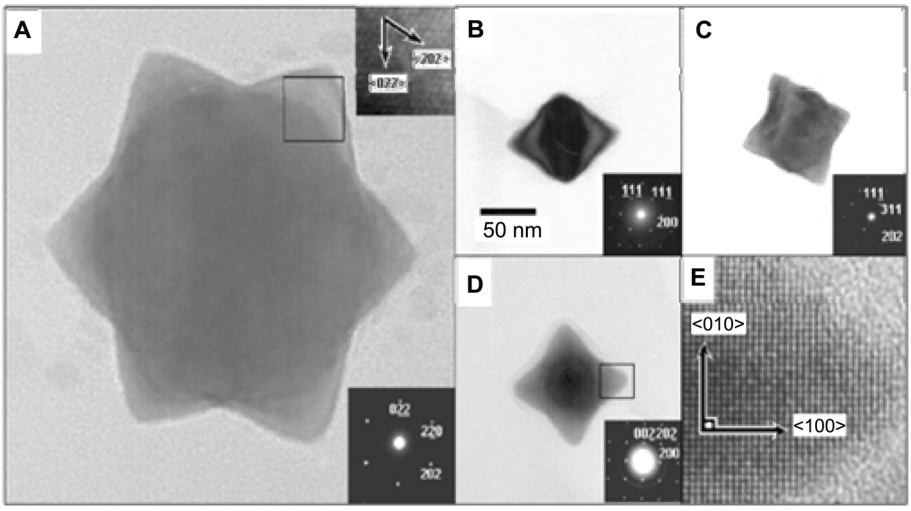

Figure 10. Star-shaped PbS nanocrystals. (A) TEM image of star-shaped PbS nanocrystals synthesized at 230 °C. (Inset) HRTEM image of lattice fringes with zone axis of [111]. (B-D) TEM images and electron diffraction patterns with zone axis of (B) [110], (C) [112], and (D) [100], respectively. (E) HRTEM image of zoomed fringes with zone axis of [100].

{100} faces. When excess thermal energy is supplied at high growth temperature (~300 °C), thermodynamic regime governs the major growth processes. In this growth regime, nearly isotropic growth from the tetradecahedron seeds is favored and therefore, cube shapes of PbS are obtained (Figure 9A, C). Under the conditions of low temperature (~140 °C) and in the presence of surface selective dodecanethiol molecules, however, the growth process shifts into the kinetic growth regime and anisotropic growth on the {100} faces with high surface energy is preferred. Remember that {111} faces are selectively stabilized under the presence of dodecanethiol molecule. This results in one-dimensional rod-based multipod structures (Figure 9B, D). HRTEM images of tadpole-shaped and cross-shaped nanocrystals prepared at 140 °C and the interplanar distance measurements indicate that the rod grows along the [001] direction from a tetradecahedron seed (Figure 9E, F). Interestingly, star-shaped nanocrystals, as a transient species between isotropic zero-dimensional and anisotropic one-dimensional shapes are obtained at an intermediate growth temperature (~180 °C) (Figure 10A). TEM and electron diffraction (ED) analyses by tilting the star-shaped nanocrystals with different zone axes reveal that the nanocrystals results from the fast growth and progressive shrinking of the {100} faces into sharp triangular corners (Figure 10B-E).

Biomedical Applications of Colloidal Nanocrystals

Since inorganic nanocrystals exhibit unique properties, the development of next generation nanosystems for the biomedical and electronic applications is highly anticipated. Especially, its small size and enhanced properties enable them to be utilized as probes and vectors for the advanced biomedical applications including sensing and imaging, separation, and therapy (Figure 11).[58] One of the representative examples is semiconductor quantum dots which exhibit tunable emitting wavelengths of light and high

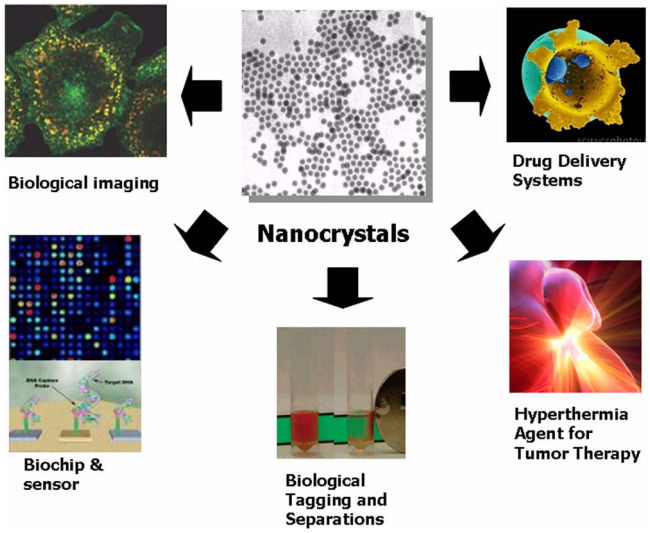

Figure 11. Possible biomedical applications of nanocrystals.

photochemical stability. Such novel properties of semiconductor quantum dots enable multiplexed detection,[59] real time observation of cell signaling,[60] near infra-red imaging,[61] and long term cell evolution,[62] which were difficulties with conventional organic dye-based fluorescence imaging techniques.

Another successful nanocrystal-based biomedical application is magnetic a nanocrystal-based nano-bio system. When magnetic nanocrystals are incorporated into biological environments, they can be utilized as a magnetic probe for detection and imaging and as a magnetic vector for cell separation and drug delivery. In particular, when they are utilized as probes in magnetic resonance imaging (MRI), it can bring significant enhancement in current biomedical imaging.[63-69] Although modern MRI is one of the most powerful medical diagnostic tools due to its non-invasive nature and multi-dimensional tomographic capabilities coupled with high spatial resolution, its temporal resolution

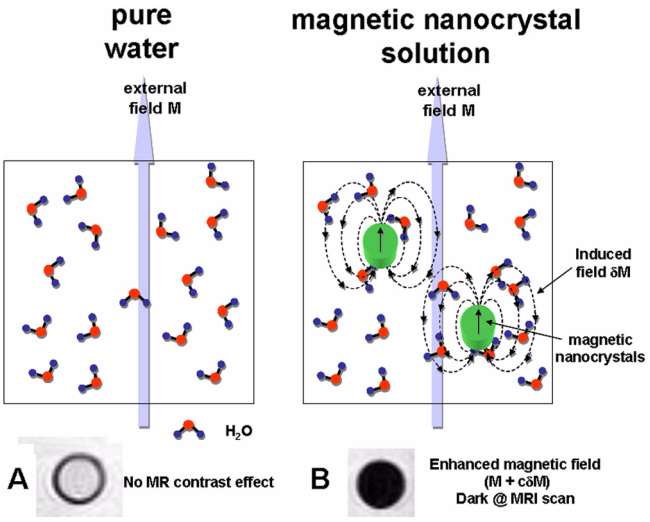

Figure 12. Magnetic resonance (MR) contrast effect of magnetic nanocrystals.

and sensitivity of MRI are still underperforming compared with other tools. However, such aspects can be significantly improved with the use of magnetic nanocrystals. Under an applied magnetic field, induced magnetic spins in magnetic nanocrystals perturb the nuclear spin relaxation processes of protons of water molecules surrounding magnetic nanocrystals. This effect leads to the shortening of spin-spin relaxation time (T2) of the proton, which results in darkening of MR images (Figure 12). When magnetic nanocrystals are conjugated with biologically active materials (*e.g.* antibody), the resulting nanocrystal-biomolecule conjugates have the multi-functionalities of both MR contrast effect of magnetic nanocrystals and selective molecular/biological recognition of target molecules. This conjugate can act as molecular imaging agents which can efficiently report molecular/genetic events of region-of-interest target tissues.

Despite such potentials of magnetic nanocrystals as molecular MR imaging agents, utilizations of magnetic nanocrystals have been mostly limited to in vitro systems with very few successful demonstrations in the in vivo systems: MRI of inflammation and infarction,[68,69] transgene expression of engineered transferrin receptors in live mice,[66] and MR detection of apoptotic cells in live rabbits and mice.[63] This is partly due to the underdevelopment and lack of suitable of bio-compatible magnetic nanocrystals. Therefore, for the successful molecular imaging, it is important to develop high performance magnetic nanocrystal systems with the capabilities of excellent magnetic properties, the ability to escape from reticuloendothelial system (RES), and possession of active functionality to be linked with biologically active molecules.

Development of Biocompatible Magnetic Nanocrystals for MR Contrast Effects and their Utilization for Cancer Detection

Since magnetic property of nanocrystals highly depends

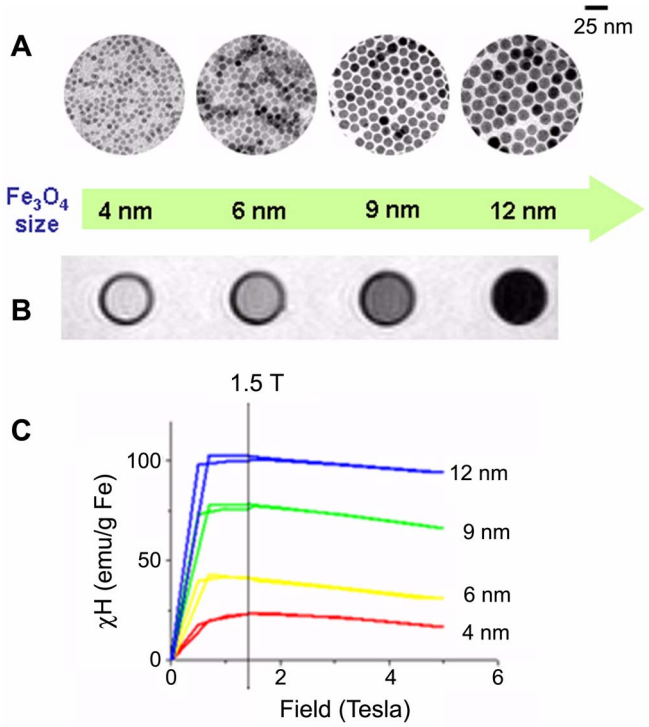

Figure 13. Nanoscale size effect of Fe_3O_4 nanocrystals. (A) TEM images of iron oxide (Fe_3O_4) nanocrystals of 4 nm, 6 nm, 9 nm, and 12 nm. (B) Size dependent T2-weighted MR images of water-soluble iron oxide nanocrystals. (C) Magnetization of water-soluble iron oxide nanocrystals measured by a SQUID magnetometer.

on the size, shape, stoichiometry, and crystallinity, it is necessary prerequisite to obtain the ability to control such materials properties. Conventional water-phase synthetic protocols generally suffer difficulties to achieve ultimate size-controllability, monodispersity, and stoichiometric composition.[70,71] In contrast, nonhydrolytic high temperature injection methods allow one to have such desired high size-controllability, highly single crystallinity, and stoichiometry control. It has been demonstrated these nonhydrolytically synthesized nanocrystals can be utilized as MR contrast agents.[72-74] Various sized iron oxide nanocrystals through high temperature injection methods including 4, 6, 9, and 12 nm with narrow size distribution ($\sigma < 8\%$) are fabricated (Figure 13A). Subsequently, 2,3-dimercaptosuccinic acid (DMSA) ligand is introduced into the nanocrystal surface,[72] which can endow them high water-phase stability through i) carboxylate chelate bonding to iron and ii) intermolecular disulfide cross-linkages between the ligands (Figure 14). Obtained water-soluble iron oxide nanocrystals exhibit excellent size-dependent magnetism and MR contrast effects. As increasing the size of nanocrystals from 4 to 6, 9, and 12 nm, the mass magnetization value at 1.5 T gradually increases from 25 to 43, 80, and 102 emu/(g Fe) (Figure 13C) and higher MR contrast effects (*i.e.* darker MR image) were seen (Figure 13B).[72]

When these nanocrystals are conjugated to the cancer targeting antibody molecules, Herceptin, the nanocrystal-Herceptin conjugates can be effectively used for breast

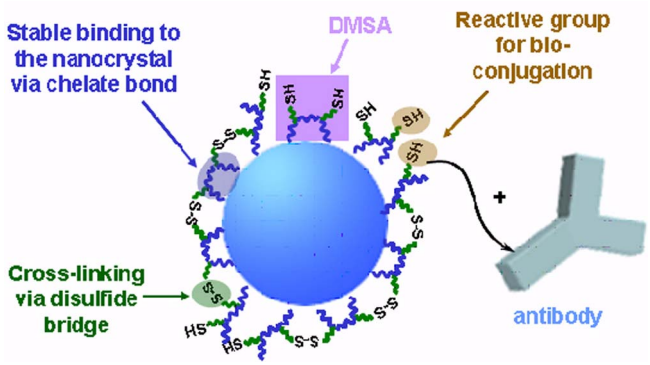

Figure 14. Schematic of 2,3-dimercaptosuccinic acid (DMSA)-coated water-soluble iron oxide nanocrystals.

cancer diagnosis.[75] The nanocrystals have high magnetic properties and very small hydrodynamic size (~10 nm), which are advantageous for both *in vitro* and *in vivo* cancer imaging. Such enhanced property enables *in vitro* detection of cancer cells with HER2/neu overexpression (SK-BR-3) (Figure 15). When these magnetic nanocrystals are utilized for *in vivo* detection of cancer cells (NIH3T6.7) implanted in mice, they successfully detected the cancer cells with high MR contrast signal in the tumor sites (Figure 16). When iron oxide-control conjugates are injected into mice, no change in the color-mapped MR signal (Figure 16A) and T2 values (Figure 16C) at the tumor site is observed. In contrast, after the injection of iron oxide-Herceptin conjugates, immediate color changes to blue is evident and a continuous T2 value

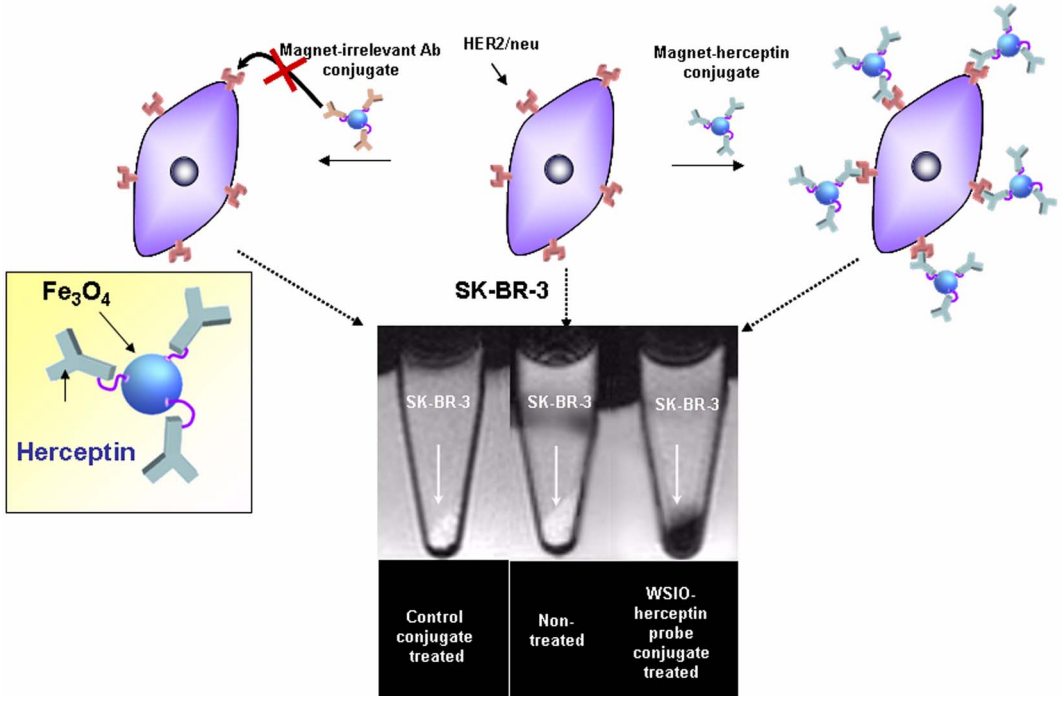

Figure 15. *In vitro* MR detection of HER2/neu overexpressed cancer cells by using magnetic iron oxide-Herceptin conjugates.

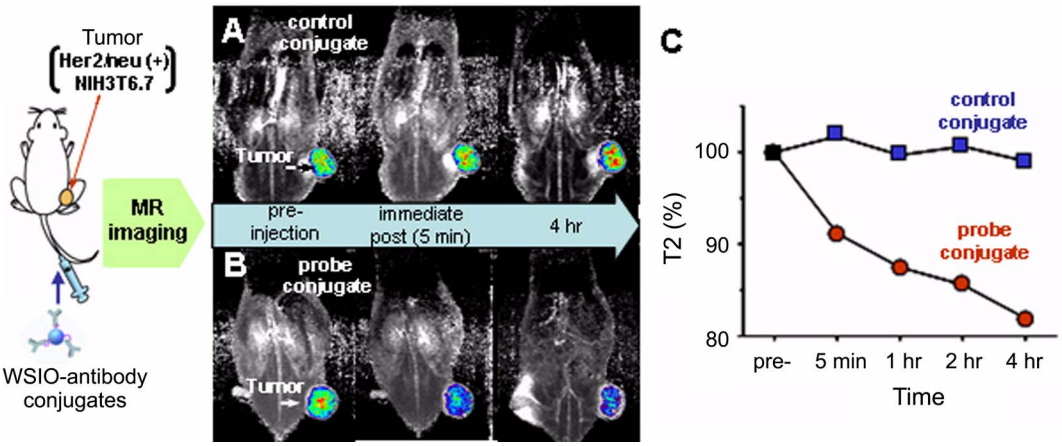

Figure 16. *In vivo* MR detection of cancer implanted in a nude mouse. Color maps of T2-weighted MR images of cancer cells (NIH3T6.7) implanted mice at the different temporal points (pre-injection, immediate post, 4h) after the intravenous injection of (A) iron oxide-antibody control conjugates and (B) iron oxide-Herceptin probe conjugates. (C) Plot of T2 values of cancer cells in (A) and (B) samples versus time after the injection of iron oxide-antibody control conjugates.

drop of ~10% is observed within 5 min and ~20% at 4h (Figure 16B, C), which implies that the iron oxide-Herceptin conjugates successfully reach and bind to the target cancer cells.

Concluding Remarks and Future Directions

Nanoscale controllability of inorganic nanocrystals can be achieved by a systematic understanding of key factors on the nanocrystal growth processes. In particular, we have discussed important shape-guiding parameters and their specific roles on the shape guiding processes. The crystalline phase of nucleation seeds, the surface energy, and the choice of crystal growth regimes are found to be crucial. These parameters can be further modulated by controlling reaction conditions such as growth temperature, the use of surface selective capping molecules, and monomer concentration.

In addition to those nanocrystals presented in this account, there have been many interesting novel shaped nanocrystals reported by others. Even for such successes of ours and others, the successful fabrications have been mostly limited to zero- and one- dimensional shapes of nanocrystals and a narrow range of materials systems. The success of this field depends heavily on the development of more versatile but reliable synthetic schemes for the tailored architectures of nanocrystals with desired components. Many new and as of yet undiscovered nanocrystals will become the key components for further scientific and technological applications. Therefore, the systematic elucidation of nanoscale physical properties of novel nanocrystals should be accompanied along with their synthetic protocols, with aspects of both theoretical and experimental approaches.

Even though nanocrystals have great potential to revolutionize current biomedical diagnosis and therapy, their successful utilizations have been very limited and is in early stages. One of the major obstacles to be resolved is the development of biocompatible nanocrystals with high colloidal stability and desired physical and chemical properties. High colloidal stability against physiological conditions and small size is the necessary prerequisites. When such biocompatible nanocrystals with optimal properties are obtained, it will be feasible to develop new nano-bio hybrid systems with multi-functional capabilities such as ultra-high detection sensitivity and therapeutic capability.

Acknowledgment. We thank KBSI for High Voltage Electron Microscopic (HVEM) and TEM analyses. This work is supported by the Korea Research Foundation (KRF-2003-041-C00172) and the BK-21 project.

References

1. Alivisatos, A. P. *Science* **1996**, *271*, 933.
2. Markovich, G. C.; Collier, P.; Henrichs, S. E.; Remacle, F.; Levine, R. D.; Heath, J. R. *Acc. Chem. Res.* **1999**, *32*, 415.
3. Jin, R.; Cao, Y.; Mirkin, C. A.; Kelly, K. L.; Schatz, G. C.; Zheng, J. G. *Science* **2001**, *294*, 1901.
4. Steigerwald, M.; Brus, L. E. *Acc. Chem. Res.* **1990**, *23*, 183.
5. Hu, J.; Odom, T. W.; Lieber, C. M. *Acc. Chem. Res.* **1999**, *32*, 435.
6. Murray, C. B.; Norris, D. J.; Bawendi, M. G. *J. Am. Chem. Soc.* **1993**, *115*, 8706.
7. Yang, P. *MRS Bull.* **2005**, *30*, 85.
8. Law, M.; Goldberger, J.; Yang, P. *Annu. Rev. Mater. Res.* **2004**, *34*, 83.
9. Bakkers, E. P. A. M.; Verheijen, M. A. *J. Am. Chem. Soc.* **2003**, *125*, 3440.
10. Goldberger, J.; He, R. R.; Zhang, Y. F.; Lee, S. W.; Yan, H. Q.; Choi, H. J.; Yang, P. D. *Nature* **2003**, *422*, 599.
11. Pan, Z. W.; Dai, Z. R.; Wang, Z. L. *Science* **2001**, *291*, 1947.
12. Kong, X. Y.; Ding, Y.; Yang, R. S.; Wang, Z. L. *Science* **2004**, *303*, 1348.
13. Saito, Y.; Matsumoto, T. *Nature* **1998**, *392*, 237.
14. Gao, P. X.; Wang, Z. L. *J. Phys. Chem. B* **2004**, *108*, 7534.
15. Kohli, P.; Martin, C. J. *Drug Deliv. Sci. Tech.* **2005**, *15*, 49.
16. Pileni, M. P. *Langmuir* **1997**, *13*, 3266.
17. Chestnoy, N.; Hull, R.; Brus, L. E. *J. Chem. Phys.* **1986**, *85*, 2237.
18. Song, Q.; Zhang, Z. J. *J. Am. Chem. Soc.* **2004**, *126*, 6164.
19. Jana, N. R.; Chen, Y.; Peng, X. *Chem. Mater.* **2004**, *16*, 3931.
20. Murray, C. B.; Sun, S.; Gaschler, W.; Doyle, H.; Betley, T. A.; Kagan, C. R. *IBM J. Res. Dev.* **2001**, *45*, 47.
21. Peng, Z. A.; Peng, X. *J. Am. Chem. Soc.* **2002**, *124*, 3343.
22. Joo, J.; Na, H. B.; Yu, T.; Yu, J. H.; Kim, Y. W.; Wu, F.; Zhang, J. Z.; Hyeon, T. *J. Am. Chem. Soc.* **2003**, *125*, 11100.
23. Jun, Y.; Lee, S.-M.; Kang, N.-J.; Cheon, J. *J. Am. Chem. Soc.* **2001**, *123*, 615.
24. Peng, X.; Manna, L.; Yang, W.; Wickham, J.; Scher, E. C.; Kadavanich, A.; Alivisatos, A. P. *Nature* **2000**, *404*, 59.
25. Manna, L.; Scher, E. C.; Alivisatos, A. P. *J. Am. Chem. Soc.* **2000**, *122*, 12700.
26. Peng, Z. A.; Peng, X. *J. Am. Chem. Soc.* **2001**, *123*, 1389.
27. Manna, L.; Million, D. J.; Miesel, A.; Scher, E. C.; Alivisatos, A. P. *Nature Mater.* **2003**, *2*, 382.
28. Tang, Z.; Kotov, N. A.; Giersig, M. *Science* **2002**, *297*, 237.
29. Cozzoli, P. D.; Manna, L.; Curri, M. L.; Kudera, S.; Giannini, C.; Striccoli, M.; Agostiano, A. *Chem. Mater.* **2005**, *17*, 1296.
30. Kim, Y.-H.; Jun, Y.; Jun, B.-H.; Lee, S.-M.; Cheon, J. *J. Am. Chem. Soc.* **2002**, *124*, 13656.
31. Ahrenkiel, S. P.; Micic, O. I.; Miedaner, A.; Curtis, C. J.; Nedeljkoic, J. M.; Nozik, A. J. *Nano Lett.* **2003**, *3*, 833.
32. Gerion, D.; Zitseva, N.; Saw, C.; Casula, M. F.; Fakra, S.; Buuren, T. V.; Galli, G. *Nano Lett.* **2004**, *4*, 597.
33. Lee, S.-M.; Jun, Y.; Cho, S.-N.; Cheon, J. *J. Am. Chem. Soc.* **2002**, *124*, 11244.
34. Lifshitz, E.; Bashout, M.; Kigel, A.; Eisen, M. S.; Berger, S. *Nano Lett.* **2003**, *3*, 857.
35. Cho, K.-S.; Talapin, D. V.; Gaschler, W.; Murray, C. B. *J. Am. Chem. Soc.* **2005**, *127*, 7140.
36. Jun, Y.; Jung, Y.; Cheon, J. *J. Am. Chem. Soc.* **2002**, *124*, 615.
37. Yin, M.; Gu, Y.; Kuskovsky, I. L.; Andelman, T.; Zhu, Y.; Neumark, G. F.; O'Brien, S. *J. Am. Chem. Soc.* **2004**, *126*, 6206.
38. Mouge, M.; Kahn, M. L.; Maisonnat, A.; Chaudret, B. *Angew. Chem. Int. Ed.* **2003**, *42*, 5321.
39. Niederberger, M.; Bartl, M.-H.; Stucky, G. D. *J. Am. Chem. Soc.* **2002**, *124*, 13642.
40. Jun, Y.; Casula, M. F.; Sim, J.-H.; Kim, S. Y.; Cheon, J.; Alivisatos, A. P. *J. Am. Chem. Soc.* **2003**, *125*, 15981.
41. Seo, J.; Jun, Y.; Ko, S. J.; Cheon, J. *J. Phys. Chem. B* **2005**, *109*, 5389.
42. Lee, K.; Seo, W. S.; Park, J. T. *J. Am. Chem. Soc.* **2003**, *125*, 3408.
43. Park, J.; Kang, E.; Bae, C. J.; Park, J.-G.; Noh, H.-J.; Kim, J.-Y.; Park, J.-H.; Park, H.-M.; Hyeon, T. *J. Phys. Chem. B* **2004**, *108*, 13594.
44. Urban, J. J.; Yun, W. S.; Gu, Q.; Park, H. *J. Am. Chem. Soc.* **2002**, *124*, 1186.
45. Cheon, J.; Kang, N.-J.; Lee, S.-M.; Lee, J.-H.; Yoon, J.-H.; Oh, S.-J. *J. Am. Chem. Soc.* **2004**, *126*, 1950.

46. Larsen, T.-H.; Sigman, M.; Ghezelbash, A.; Doty, R. C.; Korgel, B. A. *J. Am. Chem. Soc.* **2003**, *125*, 5638.
47. Ghezelbash, A.; Sigman, M.; Doty, R. C.; Korgel, B. A. *Nano Lett.* **2004**, *4*, 537.
48. Puntes, V. F.; Zanchet, D.; Erdonmez, C. K.; Alivisatos, A. P. *J. Am. Chem. Soc.* **2002**, *124*, 12874.
49. Park, J.-I.; Kang, N.-J.; Jun, Y.; Oh, S.-J.; Ri, H. C.; Cheon, J. *Chemphyschem* **2002**, *3*, 543.
50. Cao, Y. C. *J. Am. Chem. Soc.* **2004**, *126*, 7456.
51. Macintyre, J. E. *Dictionary of Inorganic Compounds*, 1st ed.; London: New York, 1992.
52. Lu, J.; Qi, P.; Peng, Y.; Meng, Z.; Yang, Z.; Yu, W.; Qian, Y. *Chem. Mater.* **2001**, *13*, 2169.
53. Zelaya-Angel, O.; Alvaradi-Gol, J. J.; Lozada-Morales, R.; Vargas, H.; Ferreira da Silva, A. *Appl. Phys. Lett.* **1994**, *64*, 291.
54. Yeh, C.-Y.; Lu, Z. W.; Froyen, S.; Zunger, A. *Phys. Rev. B* **1992**, *46*, 10086.
55. Micic, O. I.; Sprague, J. R.; Curtis, C. J.; Jones, K. M.; Machol, J. L.; Nozik, A. J.; Giessen, H.; Fluegel, B.; Mohs, G.; Peyghambarian, N. *J. Phys. Chem.* **1995**, *99*, 7754.
56. Hu, J.; Li, L.-S.; Yang, W.; Manna, L.; Wang, L.; Alivisatos, A. P. *Science* **2001**, *292*, 2060.
57. Sugimoto, T. *Monodispersed Particles*, 1st ed.; Elsevier Science: 2001.
58. Alivisatos, A. P. *Nature Biotechnol.* **2004**, *22*, 47.
59. Chan, W. C. W.; Nie, S. *Science* **1998**, *281*, 2016.
60. Lidke, D. S.; Nagy, P.; Heintzmann, R.; Arndt-Jovin, D. J.; Post, J. N.; Grecco, H. E.; Jares-Erijman, E. A.; Jovin, T. M. *Nature Biotechnol.* **2004**, *22*, 198.
61. Kim, S. *et al. Nature Biotechnol.* **2004**, *22*, 93.
62. Dubertret, B.; Skourides, P.; Norris, D. J.; Noireaux, V.; Brivanlou, A. H.; Libchaber, A. *Science* **2002**, *298*, 1759.
63. Zhao, M.; Beauregard, D. A.; Loizou, L.; Davletov, B.; Brindle, K. M. *Nature Med.* **2001**, *7*, 1241.
64. Kang, H. W.; Josephson, L.; Petrovsky, A.; Weissleder, R.; Bogdanov Jr., A. *Bioconj. Chem.* **2002**, *13*, 122.
65. Artemov, D.; Mori, N.; Okollie, B.; Bhujwalla, A. M. *Magn. Reson. Med.* **2003**, *49*, 403.
66. Weissleder, R.; Moore, A.; Mahmood, U.; Bhorade, R.; Benveniste, H.; Chiocca, E. A.; Basilion, J. P. *Nature Med.* **2000**, *6*, 351.
67. Perez, J. M.; Josephson, L.; O'Loughlin, T.; Hogemann, D.; Weissleder, R. *Nature Biotechol.* **2002**, *20*, 816.
68. Weissleder, R.; Lee, A. S.; Khaw, B. A.; Shen, T.; Brady, T. J. *Radiology* **1992**, *182*, 381.
69. Weissleder, R.; Lee, A. S.; Fischman, A. J.; Reimer, P.; Shen, T.; Wilkinson, R.; Callahan, R. J.; Brady, T. J. *Radiology* **1991**, *181*, 245.
70. Fauconnier, N.; Pons, J. N.; Roger, J.; Bee, A. *J. Colloid Interface Sci.* **1997**, *194*, 427.
71. Shen, T.; Weissleder, R.; Papisov, M.; Bogdanov, A. Jr.; Brady, T. *Mag. Reson. Med.* **1993**, *29*, 599.
72. Jun, Y.; Huh, Y.-M.; Choi, J.; Lee, J.-H.; Song, H.-T.; Kim. S.; Yoon, S.; Kim, K.-S.; Shin, J.-S.; Suh, J.-S.; Cheon, J. *J. Am. Chem. Soc.* **2005**, *127*, 5732.
73. Huh, Y.-M.; Jun, Y.; Song, H.-T.; Kim, S.; Choi, J.-s.; Lee, J.-H.; Yoon, S.; Kim, K.-S.; Shin, J.-S.; Suh, J.-S.; Cheon, J. *J. Am. Chem. Soc.* **2005**, *127*, 12387.
74. Veiseh, O.; Sun, C.; Gunn, J.; Kohler, N.; Gabikian, P.; Lee, D.; Bhattarai, N.; Ellenbogen, R.; Sze, R.; Hallahan, A.; Olson, J.; Zhang, M. *Nano Lett.* **2005**, *5*, 1003.
75. Hudziak, R. M.; Lewis, G. D.; Winget, M.; Fendly, B. M.; Shepard, H. M.; Ullrich, A. *Mol. Cell Biol.* **1989**, *9*, 1165.